JGR Oceans

RESEARCH ARTICLE
10.1029/2020JC016297

Key Points:
- Niño3.4 SST trends are positive in all reanalysis products, but zonal SST gradient trends do not agree with each other
- Zonal SST gradient in two reanalysis products is strengthening, but the ocean dynamic drivers are different
- Suitability of ocean reanalysis products must be verified for the intended study, ensuring that their biases do not affect the conclusions

Supporting Information:
- Supporting Information S1

Correspondence to:
T. I. Eldho,
eldho@civil.iitb.ac.in

Citation:
Jayasankar, T., Murtugudde, R., & Eldho, T. I. (2020). Inconsistent atmosphere-ocean dynamics and multidecadal zonal SST gradient trends across the equatorial Pacific Ocean in reanalysis products. *Journal of Geophysical Research: Oceans*, *125*, e2020JC016297. https://doi.org/10.1029/2020JC016297

Received 5 APR 2020
Accepted 13 AUG 2020
Accepted article online 18 AUG 2020

Inconsistent Atmosphere-Ocean Dynamics and Multidecadal Zonal SST Gradient Trends Across the Equatorial Pacific Ocean in Reanalysis Products

T. Jayasankar[1], R. Murtugudde[1,2,3], and T. I. Eldho[1,2]

[1]Interdisciplinary Programme in Climate Studies, Indian Institute of Technology, Bombay, India, [2]Department of Civil Engineering, Indian Institute of Technology, Bombay, India, [3]ESSIC, University of Maryland, College Park, MD, USA

Abstract Ocean reanalysis products are routinely employed as reality checks in model evaluations and for process studies. This is especially so for critical regions such as the equatorial cold tongue (ECT) in the eastern equatorial Pacific where models suffer a chronic cold bias. ECT is a major player in the Pacific equatorial zonal sea surface temperature (SST) gradient (Δ_{EW}SST) that has a significant impact on oceanic heat uptake and thus global climate. Hence, we investigate the reliability of three ocean reanalysis products for surface flux and ocean dynamic controls on Δ_{EW}SST and Niño3.4 SST trends. We infer that while Niño3.4 SST trends are positive in all products, the signs of Δ_{EW}SST trends do not agree with each other because initial conditions likely play a big role in their evolution. However, for Δ_{EW}SST trends, the effect of initial conditions gets canceled out to some extent. Mixed layer heat budget and trends in ocean dynamic features such as tropical and subtropical cells, equatorial undercurrent, and subsurface temperatures are also diagnosed. We show that two reanalysis products that show a strengthening of Δ_{EW}SST have contradicting trends in their surface heat flux and ocean dynamic contributions. This suggests that without accurate surface heat and momentum fluxes, data assimilation techniques may produce an east–west trend that is inconsistent among each other. Reanalysis products must address these issues considering the importance of this gradient.

Plain Language Summary The east to west sea surface temperature (SST) gradient (Δ_{EW}SST) of the equatorial Pacific Ocean (EQPO) is characterized by a highly variable cold SST over the eastern EQPO and relatively less variable warm, fresh pool in the west. This gradient reinforces the equatorial easterlies because of a positive feedback with wind-driven upwelling in the east. Anomalous weakening (strengthening) of the Δ_{EW}SST and the resulting weaker (stronger) easterlies lead to an El Niño (La Niña). On climate change timescales, this feedback modulates oceanic heat uptake and atmospheric warming as seen by the La Niña-like state during 1998 to 2013 and the so-called global warming pause. The reliability of future climate projections depends on simulating the coupled dynamics of the region faithfully due to its global reach. Therefore, climate models have to be thoroughly evaluated. As observations are insufficient, ocean reanalysis products, which are comprehensive records produced by merging observations and models, serve as surrogates for observations in this context. However, the surface heat fluxes and ocean dynamics are inconsistent among three reanalysis products analyzed. The inconsistencies in surface fluxes in two products still produce a similar Δ_{EW}SST trend but with different ocean dynamic pathways.

1. Introduction

The eastern equatorial Pacific (EEP) is characterized by persistent cold sea surface temperatures (SSTs) which soak up heat from the atmosphere, while the western equatorial Pacific (WEP) is home to some of the warmest SSTs and persistent atmospheric deep convection. This east–west SST gradient plays a critical role in the coupled ocean-atmosphere feedbacks (Bjerknes, 1969) during El Niño Southern Oscillation (ENSO). Much debate in the last two decades has focused on the potential role of this SST gradient in modulating the global temperature trend (e.g., Cane et al., 1997; Collins et al., 2010; Delworth et al., 2015; Karnauskas et al., 2009; Seager & Murtugudde, 1997; Trenberth et al., 1998). It has served as the poster child for the extensive debate on the causes for the recent global warming pause (England et al., 2014; Kosaka & Xie, 2013; Lee et al., 2015). This gradient is maintained by the trade winds that drive an Ekman divergence

and upwelling in the east and drag the surface waters westward. This results in a warm pool with higher sea level and deeper thermocline in the western Pacific. The east–west SST gradient and the associated positive feedback underlie the debate on modulation of global warming and oceanic heat uptake as well as the response of ENSO itself to global warming (Collins et al., 2010; Vecchi & Wittenberg, 2010).

Advances in observing and modeling the global climate have been impressive (Simpkins, 2017). However, one major shortcoming of CMIP5 models is an excessively cold equatorial cold tongue (ECT; known as cold tongue bias). This is due to biases in winds driven by ocean response to a precipitation deficit through Bjerknes feedback (Li & Xie, 2014). Some studies (Clement et al., 1996; Seager & Murtugudde, 1997; Sun & Liu, 1996) suggest an increasing Δ_{EW}SST in response to global warming pushing the system toward a climatology favoring strong La Niñas and weak El Niños. However, the future of ENSO in a warming world remains an open question (Cai et al., 2018). The climatological upwelling in the ECT is a critical process for the evolution of Δ_{EW}SST considering the expected continuation of the warming in the WEP. Consequently, the feedback mechanism can be expected to enhance the Δ_{EW}SST further, and this expectation is backed by observations (Cane et al., 1997; Karnauskas et al., 2009) even though the lack of sufficient observations is always a caveat (Vecchi et al., 2008). However, unlike observations and ocean reanalysis products (Ocean Reanalysis System 4 [ORAS4]), CMIP5 models predict a weakening Δ_{EW}SST (Coats & Karnauskas, 2018; Seager et al., 2019) favoring strong El Niños. With the possible influence of natural variability on this bias in trends ruled out, the posited origin of this bias in trend is the cold tongue bias (Seager et al., 2019). Model-dependent causes for the cold tongue bias also include anomalously strong/deep upwelling, strong anomalies in equatorial thermocline depths, strong anomalies in cloud shading/evaporation, errors in depth of shortwave penetration, and weak lateral stirring and vertical mixing due to tropical instability waves and eddy-induced advection (Ray et al., 2018b). Ray et al. (2018a, 2018b) discuss a framework for the evaluation of CMIP6 models using observations and reanalysis products. The study highlights the significance of the mixed layer (ML) heat budget analysis of the equatorial Pacific for the evaluation, especially of the ECT. It also underscores the need for evaluating climate models based on ocean dynamic (OD) processes beyond simple indices such as SSTs and thermocline depths. This demands robust observations and reliable reanalysis products. At this juncture, this raises an important question that cannot be dodged: just how reliable are ocean reanalysis products?

In order to answer this question, we investigate three reanalysis products (ORAS4, German contribution to the consortium for Estimating the Circulation and Climate of the Ocean 2 [GECCO2], and Ensemble Coupled Data Assimilation system by Geophysical Fluid Dynamics Laboratory [GFDL]) in the context of seasonal and decadal trends in Δ_{EW}SST (Karnauskas et al., 2009), Niño3.4 SST trends (Seager et al., 2019), ML heat budget, and upper layer ODs. We show that there is no consensus between the three reanalysis products studied in the context of Δ_{EW}SST trends. Most notably, two products which show a strengthening of Δ_{EW}SST have contradicting trends in their ODs. The following sections illuminate the differences among reanalysis products and their causes. The results presented in this manuscript should serve as a warning against blindly relying on ocean reanalyses in evaluating climate models or in advancing process understanding.

2. Data and Methods

2.1. Data

The ocean reanalysis products studied are the ORAS4 (Balmaseda et al., 2013), GECCO2 (Kohl, 2015), and GFDL (Chang et al., 2013). ORAS4 is forced with the European Centre for Medium-Range Weather Forecasts (ECMWF) products (ERA-40 until 1978, Uppala et al., 2005; ERA-Interim from 1979 onwards, Dee et al., 2011). GECCO2 and GFDL are forced with the National Centers for Environmental Prediction (NCEP) surface fluxes. GECCO2 is forced with the adjusted NCEP/National Center for Atmospheric Research (NCAR) (Kalnay et al., 1996) fluxes alone. However, GFDL is a coupled climate model system where the first guess for the atmospheric heat fluxes (HFs) is model generated, but it is constrained by NCEP reanalysis fluxes through data assimilation. As the HFs used in GFDL are not available, in this study, we associate GFDL to the available NCEP fluxes (NCEP/NCAR until 1978 and NCEP/Department of Energy (DOE) fluxes after 1978, Kanamitsu et al., 2002).

Four observational SST data sets are also analyzed to elicit the observed trends in the equatorial Pacific SSTs. They are the UK Hadley Center Global Sea Surface Temperature Version 3 (HadISST; Kennedy et al., 2011a, 2011b), National Oceanic and Atmospheric Administration Extended Reconstructed SST version 5 (ERSST; Huang et al., 2017), Kaplan extended SST Version 2 (Kaplan SST; Kaplan et al., 1998), and Japan Meteorological Agency, Characteristics of Global SST Analysis Data Version 2 (COBE2; Hirahara et al., 2014). The respective horizontal resolutions of HadISST, ERSST, Kaplan SST, and COBE2 are 1°, 2°, 5°, and 1°.

2.2. Methodology

In this study, we first compare decadal trends and season-wise trends of Δ_{EW}SST and Niño3.4 SST. Δ_{EW}SST is computed by subtracting EEP (5°S to 5°N, 230–280°E) SST from WEP (5°S to 5°N, 150–200°E) SST as given in Karnauskas et al. (2009). The Niño3.4 SST is computed over 190–240°E and 5°S to 5°N as in Seager et al. (2019). All trends estimated in this study are the Theil-Sen (Sen, 1968; Theil, 1950) slope, and the decadal components are computed using an 8-year moving window smoothing (using smooth function, a curve fitting tool available in MATLAB). All slope and mean estimates are for the period of 1961 to 2010 unless specified otherwise. The aforementioned analysis period is chosen as GFDL reanalysis is only available from 1961 and GECCO2 reanalysis is restarted with new initial conditions after 2010. To understand the surface HF and OD contributions to SST trends, a heat budget analysis of the ML is carried out.

As per Ray et al. (2018a), for such evaluations, ML should not be too deep such that the ML mean temperature reflects the SST and ML heat budget analysis represents the mechanisms that modulate the SST. However, ML also should be deep enough to absorb most of the downward shortwave flux. Investigations by Ray et al. (2018a) show that ML depth defined by the critical density criteria of a difference of 0.125 kg/m^3 between potential densities of the surface layer and ML bottom layer satisfies the conditions for heat budget analysis the best. The formulations for ML heat budgeting (Equations 1, 2, 3 and 4) is based on Hendon (2003) and Dong et al. (2007).

$$\frac{\partial T_h}{\partial t} = \frac{Q_{net} - q(-h)}{\rho_0 C_p h} + \frac{\partial T_h}{\partial t}_{OD} \tag{1}$$

$$q(-h) = q(0)\left[Re^{\left(-\frac{h}{\gamma 1}\right)} + (1-R)e^{\left(-\frac{h}{\gamma 2}\right)}\right] \tag{2}$$

$$\frac{\partial T_h}{\partial t}_{OD} = \frac{1}{h}\int_{-h}^{0}\left(-u\frac{\partial T}{\partial x} - v\frac{\partial T}{\partial y}\right)dz - w_e\frac{\Delta T}{h} + \frac{\partial T_h}{\partial t}_{residual} \tag{3}$$

$$w_e = \left[\frac{\partial h}{\partial t} + h\frac{\partial U_h}{\partial x} + h\frac{\partial V_h}{\partial y}\right]H \tag{4}$$

The left hand side of Equation 1 gives the rate of change of ML mean temperature where T_h is the mean ML temperature and t is time. The first term of the right hand side of Equation 1 represents the HF contribution to the ML temperature change where Q_{net} is the net surface HF into the ocean; $q(-h)$ the downward shortwave HF at the base of the ML; h depth of ML; and ρ_0 reference density of seawater and C_p its specific heat. The second term represents the net OD contribution to ML temperature tendency. Equation 2 corresponds to the downward shortwave radiation at ML base, assuming it reduces exponentially from the surface to depth h (Murtugudde et al., 2002; Paulson & Simpson, 1977; Qiu & Kelly, 1993) where $q(0)$ is the downward surface shortwave flux and the remaining terms R, $\gamma 1$, and $\gamma 2$ are constants that depend on water properties specified (Jerlov, 1968). Equation 3 represents various terms in the OD component. The first term represents the horizontal advection where, u and v are zonal (x, directed east) and meridional (y, directed north) velocities, respectively. The vertical direction is denoted by z and T is the temperature at (x, y, z) at time t. The second term represents the vertical entrainment, and w_e is the entrainment velocity. The remaining term is a residual term that also accounts for the vertical and horizontal mixing. Equation 4 gives the expansion of w_e where U_h and V_h are mean zonal and horizontal velocities of the ML. H is a Heaviside function that returns 1 when terms inside the square bracket are positive and returns 0 otherwise.

To verify the contribution by ODs to long-term ML temperature tendencies derived based on the ML heat budget, the trends in tropical and subtropical cells (TCs and STCs) are evaluated by assessing the upper

layer meridional overturning stream function. The stream function on a latitude-depth plane is computed by integrating the meridional mass flux at its zonal section from east to west followed by surface to the depth of interest. Hence, a counterclockwise (clockwise) stream function would be negative (positive) with southward (northward) flowing surface layers and northward (southward) flowing subsurface layers.

3. Trends in Equatorial Pacific SSTs and the Heat Budget

3.1. Trends in Zonal SST Gradient and Niño3.4 SST

We compare the trends in Niño3.4 SST and Δ_{EW}SST of the reanalysis products against observations as they are both key indicators of the tropical Pacific climate, especially Δ_{EW}SST which plays a significant role in the ocean-atmosphere feedbacks with a global reach (Figures 1a–1d). At interannual timescales, the products satisfactorily reproduce SSTs and the Δ_{EW}SST with slight departures in GECCO2 (Figure S1). At decadal timescales, unlike ORAS4, GFDL, and observations, the Δ_{EW}SST trend in GECCO2 is strongly negative (Figure 1d). Among observations, HadISST shows a strong positive trend in Δ_{EW}SST while other SST products show weak and insignificant trends. For Niño3.4 region, HadISST shows a weak and insignificant warming while all three reanalysis products and observations depict an increasing SST (Figure 1b). Also, among observations, the spatial patterns of SST trend show noticeable inconsistencies (Figure 2) that are concentrated along the eastern (eastward of 230°E, i.e., 130°W) equatorial Pacific (Figure 2f). Among the reanalysis products, spatial patterns of SST trends in ORAS4 match well with the observations, especially the ensemble mean of the SST products (Figure 2c). The distinct features of SST trend patterns marked by boxes A, B, C, and D in Figure 2c are well captured by ORAS4. In this regard, GFDL and GECCO2 fail to satisfactorily capture these features. The correlation between SSTs of reanalyses and observational products also underscores higher credibility of ORAS4 over the other two products (Figure S2 and Text S2). There is an exceptionally strong eastern Pacific warming trend in GECCO2 (Figures 1c and 2h). The decreasing Δ_{EW}SST in GECCO2 is due to its comparatively strong warming in EEP (Figure 1c). This is also reflected in its Niño3.4 SST trend which is the strongest among the three products. However, reanalyses (ORAS4 and GFDL) that predict a weak warming in EEP with an increasing Δ_{EW}SST also show increasing Niño3.4 SST though it is comparatively weak. This implies that while CMIP5 models are shown to overpredict the Niño3.4 SST trends (Seager et al., 2019), their Δ_{EW}SST could be different from each other. However, in the reanalysis products evaluated, the biases in initial conditions that are uniform over the basin could play a major role in their respective Niño3.4 SST trends; reanalyses approach observations with time (Figure 1b). Such systematic biases could get canceled in Δ_{EW}SST, and hence, Δ_{EW}SST could be a better indicator while diagnosing the trends in equatorial Pacific climate. It is interesting to note that in all four observational products, the trend in Niño3.4 SST is not as strong as their respective warming trends in WEP SST and EEP SST. Hence, weak warming of Niño3.4 SST in comparison with EEP and WEP SSTs could be an indication of robust ODs in the model for the analysis period.

The seasonal means and trends of Δ_{EW}SST are strongly influenced by SST variations in the EEP where upwelling and heat uptake are important (Clement et al., 1996; Karnauskas et al., 2009). Consequently, it is important to examine the seasonality of climatology and of trends in the reanalysis products. The seasonal cycle and trends of Δ_{EW}SST are well represented except in GECCO2 (Figures S3b and S3d). The climatological seasonal cycle of Δ_{EW}SST is in effect the inverse of that of the EEP SST (Figure S4b) due to its strong seasonal cycle compared to that of the WEP. Also, the trends for all months of EEP and WEP SSTs in ORAS4 and GFDL are within the range of observations. For GECCO2, the trends for each month of EEP and WEP SSTs are respectively higher and lower than the observations (Figures S4c and S4d). Despite reproducing the climatology of Niño3.4 SST well, the reanalysis products do not capture the seasonality of the trends. In particular, the cooling trend during winter months is not captured (except for ORAS4) and the warming trends at other times are much (slightly) stronger than observations in GECCO2 (ORAS4 and GFDL) (Figure S3c). To better understand the role of atmosphere-ocean dynamics in the SST trends discussed thus far, a heat budget analysis of the ML is presented next.

3.2. ML Heat Budget

The trends in ML mean temperature of the key locations (Figures 3a–3c) closely correspond to (differences within 10%) their respective SST trends (Figures 1a–1c). Since SST trends are negligible at all locations compared to the magnitude of trends in HF contributions (Figures 3d–3f), the trends in OD contributions

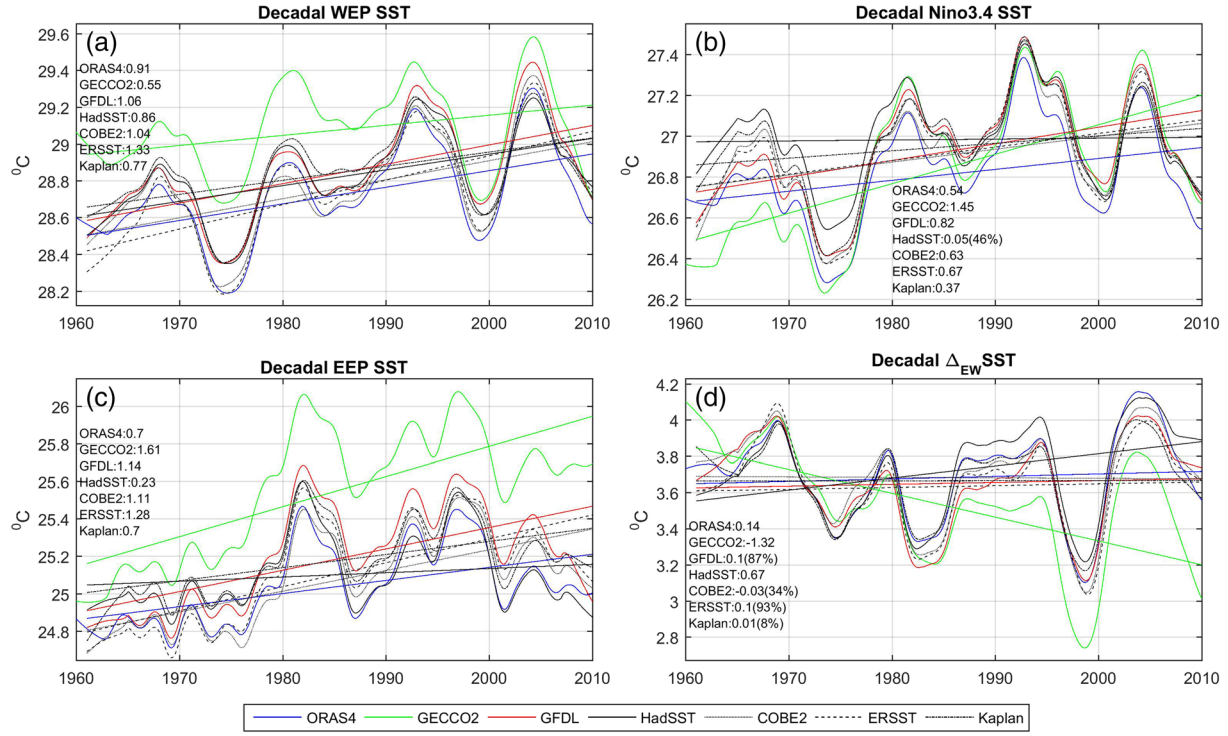

Figure 1. Smoothed (8 year) time series of (a) WEP SST, (b) Niño3.4 SST, (c) EEP SST, and (d) Δ_{EW}SST in reanalysis products and observations with trends included (significance less than 95% are also listed).

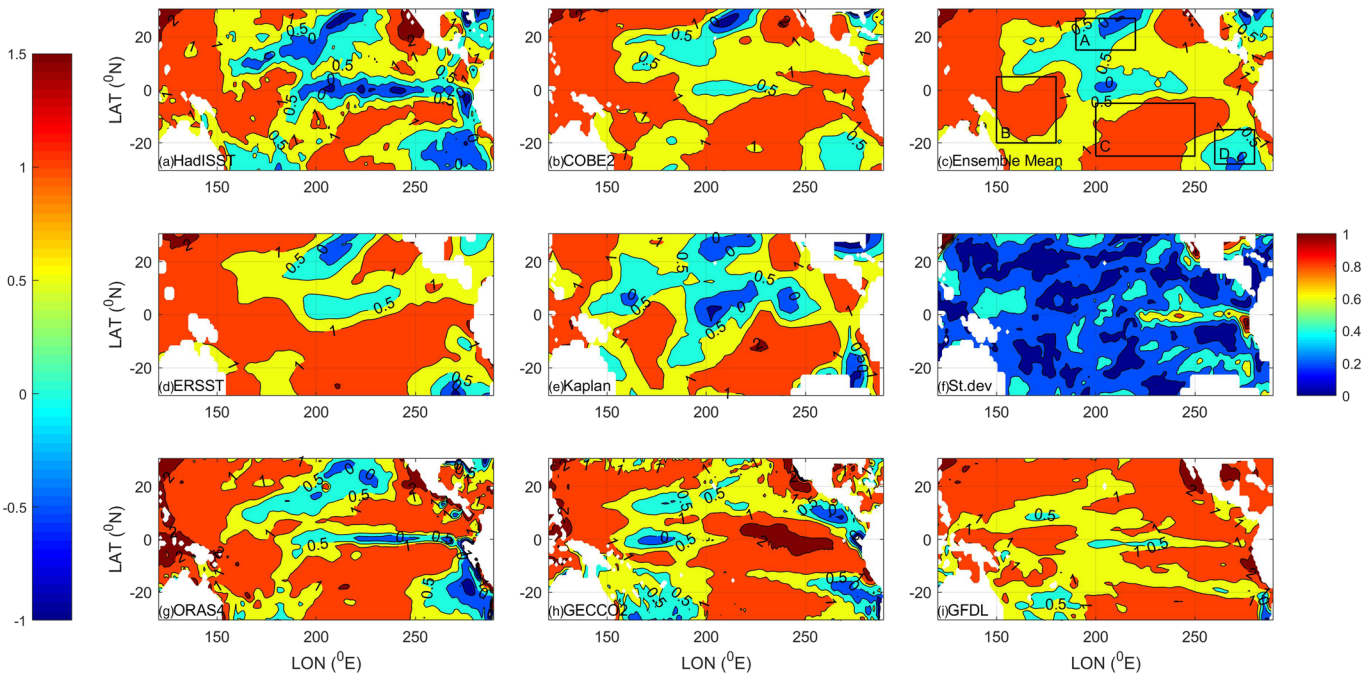

Figure 2. Spatial patterns of SST trends in (a) HadISST, (b) COBE2, (d) ERSST, (e) Kaplan SST, (g) ORAS4, (h) GECCO2, and (i) GFDL. (c) Ensemble mean and (f) standard deviation of trends in observational SST products shown in (a), (b), (d), and (e).

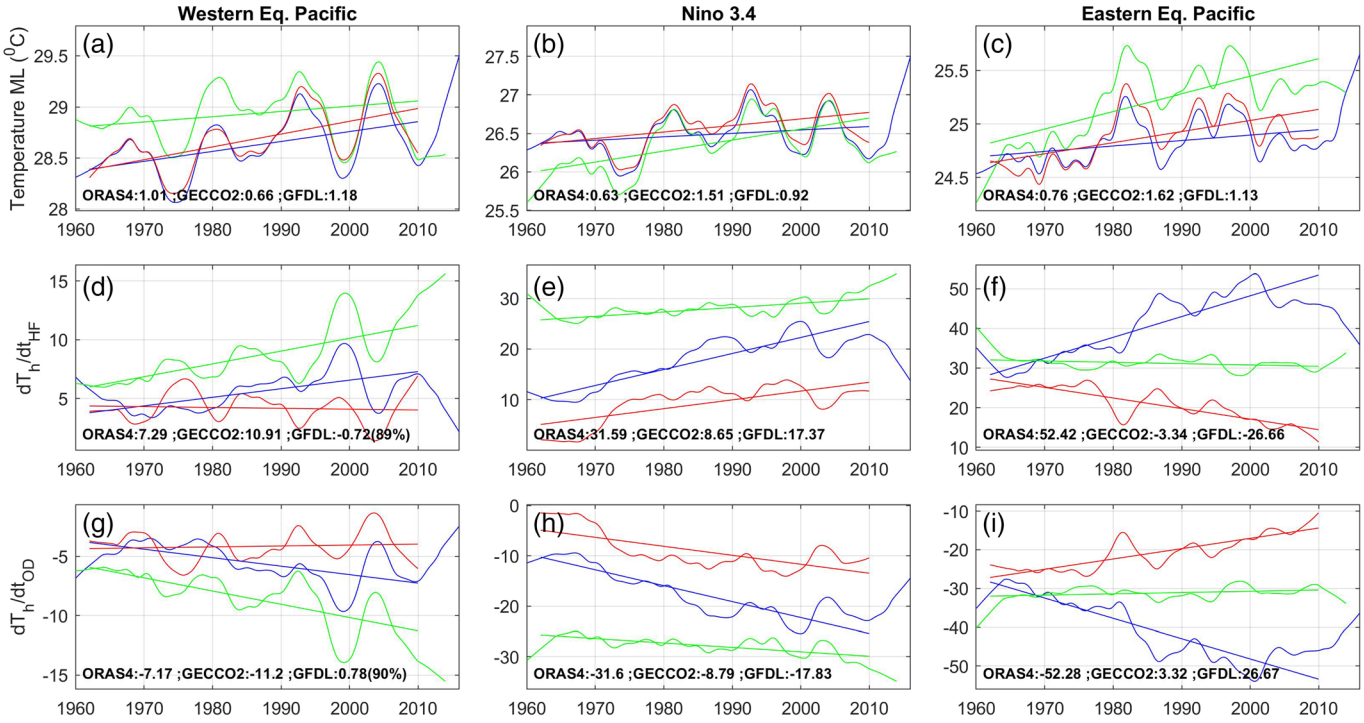

Figure 3. Smoothed (8 year) time series of ML temperature at (a) WEP, (b) Niño3.4, and (c) EEP and smoothed time series of ML temperature tendencies due to heat flux at (d) WEP, (e) Niño3.4, and (f) EEP, in reanalysis products with trends included (significance less than 95% is also included). (g–i) are the same as (d–f) but for ocean dynamic contributions.

(Figures 3g–3i) are nearly opposite to the respective trends in HF contributions. There is a consensus between the three reanalysis products when trends in their HF and OD contributions over the Niño3.4 region are compared. However, there is no consistency when trends in HF contributions in each reanalysis products at the three key locations are compared against each other (Figures 3d–3f). The HF contributions in GFDL are decreasing in both WEP and EEP. The HF contributions of GFDL and ORAS4 are based on fluxes obtained from National Oceanic and Atmospheric Administration (NOAA) and ECMWF websites, respectively, as HFs of these products are not archived along with the model outputs as in the case of GECCO2. The decreasing trend in HF contributions in GFDL shown here is due to the shift in its means when the source of HFs is switched from NCEP/NCAR fluxes to NCEP/DOE fluxes after 1978. This is depicted as a shift around 1978 in HFs of GFDL and it is clearly noticeable as changes in mean HF values of the two products (Figure S5). For the analysis period from 1961 to 2010, in ERA40 and NCEP/NCAR surface, HFs are increasing. In ORAS4, even after switching from ERA40 to ERA interim after 1978, the trends in surface HFs are increasing. Due to the non-availability of exact HFs that are used to drive the model, we are unable to report how the HFs are nudged in GFDL. In GECCO2, the trends in its net surface HFs which are adjusted before model integration are stronger than that of the respective NCEP/NCAR fluxes except for EEP (Figures S5a–S5c). In GECCO2, the trends in HF contributions in EEP are weak compared to that of ORAS4 and GFDL. However, the EEP SST trend is the strongest in GECCO2 compared to that of ORAS4 and GFDL. This suggests that the EEP cooling due to OD contributions in GECCO2 should be really weak as shown in Figure 3i. However, for ORAS4, despite having the strongest warming trend in HF contributions in EEP, its SST trends are the weakest. This suggests that the cooling trends due to OD contributions to EEP SST are strong in ORAS4 and weak in GECCO2. However, in GFDL, the declining trends in HF contribution over EEP SST suggest that OD could possibly be contributing to the warming of EEP provided that the HF trends shown in Figure 3 are more or less valid against the real fluxes forcing the product. The decomposition of OD contributions into its components (Equation 3 and Figure S6) suggests that the residual term is the major contributor in the EEP. It must be noted that this residual term also includes mixing which cannot be quantified here since

this information is not provided by the reanalysis products. This is consistent with Ray et al. (2018a) where vertical mixing is shown to be the driver in EEP SST cooling. This is because ML depth criterion chosen results in a comparatively thinner ML and layers where temperature tendencies are significantly contributed by advection is below the chosen ML (Ray et al., 2018a). Since confirming the trends in OD contributions is vital for further analysis and interpretations, we proceed to the comparison of trends in the other OD features such as the equatorial undercurrent (EUC), TCs and STCs, and subsurface temperatures that largely determine the equatorial ODs.

4. ODs in the Equatorial Pacific Ocean

4.1. Subtropical and Tropical Cells and the Equatorial Undercurrent

As per some of the previous studies (England et al., 2014; McPhaden & Zhang, 2002, 2004), the ODs of the equatorial Pacific that drive low-frequency modulations of the EEP SST and thus the Δ_{EW}SST mainly consist of TCs and STCs and the EUC which are driven by the easterlies over the basin. The Pacific STCs are upper layer meridional overturning cells within the thermocline in both hemispheres that subduct (upwell) in the subtropics (tropics) with equatorward (poleward) subsurface (surface) transport (Liu, 1994; McCreary & Lu, 1994). Additionally, in both hemispheres, narrow cells known as TCs are also present within a 5° latitude limit (Lohmann & Latif, 2005; Lu et al., 1998). The STCs determine the meridional heat transport and equatorial SSTs, thereby playing a critical role in the low-frequency variability of the equatorial Pacific (McPhaden & Zhang, 2002; Yamanaka et al., 2015). The EUC is an eastward-flowing subsurface current which is driven by the east–west pressure gradient created by sea level slope maintained by the easterlies (Drenkard & Karnauskas, 2014). The EUC along with the equatorial westward surface flow driven by the climatological easterlies thus more or less closes the equatorial zonal circulation (see Figure 3 of England et al., 2014). Hence, the strength of EUC is an indication of the strength of upwelling in EEP and the consequent cooling there.

The mean strength of the STCs and TCs along with the EUC are shown in Figures 4a–4f. The northern STC (NSTC) and northern TC (NTC) in GFDL are the strongest. The NSTC in GECCO2 is slightly stronger than that of ORAS4. The NTC in GECCO2 is the weakest. Also, the mean westward flow of the northern Pacific is weaker in GECCO2 compared to the other two (Figure 4d). The EUC is strongest in GFDL and weakest in GECCO2. Consistent with these, the easterly wind stress in GFDL are significantly stronger than that of ORAS4 and GECCO2 (Figures 4g and 5). In the eastern Pacific, especially in the Northern Hemisphere, the zonal wind stress in GFDL is nearly twice as strong as that of ORAS4 and GECCO2 (Figure 4g). This explains the comparatively stronger NTC, NSTC, and EUC in GFDL. In the Southern Hemisphere, the TC and STC in GFDL are combined to form a larger cell. However, the structure of the TCs, STCs, and EUC as well as the seasonal climatology of these cells (Figure S7) in general is consistent in the three reanalysis products with differences in their magnitudes. To elicit the trends in OD contribution to SST, the trends in STCs and EUC need to be investigated. However, we first investigate the trends in zonal wind stress used in the three products (Figure 5).

Though the spatial patterns of mean zonal wind stress are similar in all three products, the magnitude of winds in GFDL is stronger than that of ORAS4 and GECCO2 in a few regions, especially in the northern Pacific (around 10°N) and southwestern Pacific (around 20°S). As mentioned earlier, this explains the stronger STCs in GFDL. The trends in zonal wind stress in the three products are different (Figures 5d–5f). In ORAS4, the trends suggest a strengthening of easterlies all over the basin (especially so in the southern Pacific) except for the equatorial Niño3.4 region and its vicinity. Hence, in ORAS4, a strengthening of STCs and the EUC facilitating a strong cooling by upwelling in EEP can be expected. In GECCO2, the trends in wind stress are comparatively weaker, and hence, only weak trends in OD contributions are expected, if at all. In GFDL, a noticeable weakening of easterlies is observed especially in the northeastern Pacific. Hence, in GFDL, the weakening of STCs and EUC can be expected. Thus, the trends in zonal winds stress in all three products underlie the inferences drawn out of ML heat budget analysis.

To confirm the inferred trends in OD contributions to SST, we further investigate the trends in STCs and EUCs along with trends in equatorial subsurface temperature (Figure 6). In ORAS4, there is a strengthening (weakening) of southern STC (TC). Also, there is a strengthening of the NTC and a more or less stable NSTC (Figure 6a). In GFDL, the southern STC is more or less stable. However, there is a strengthening of both the

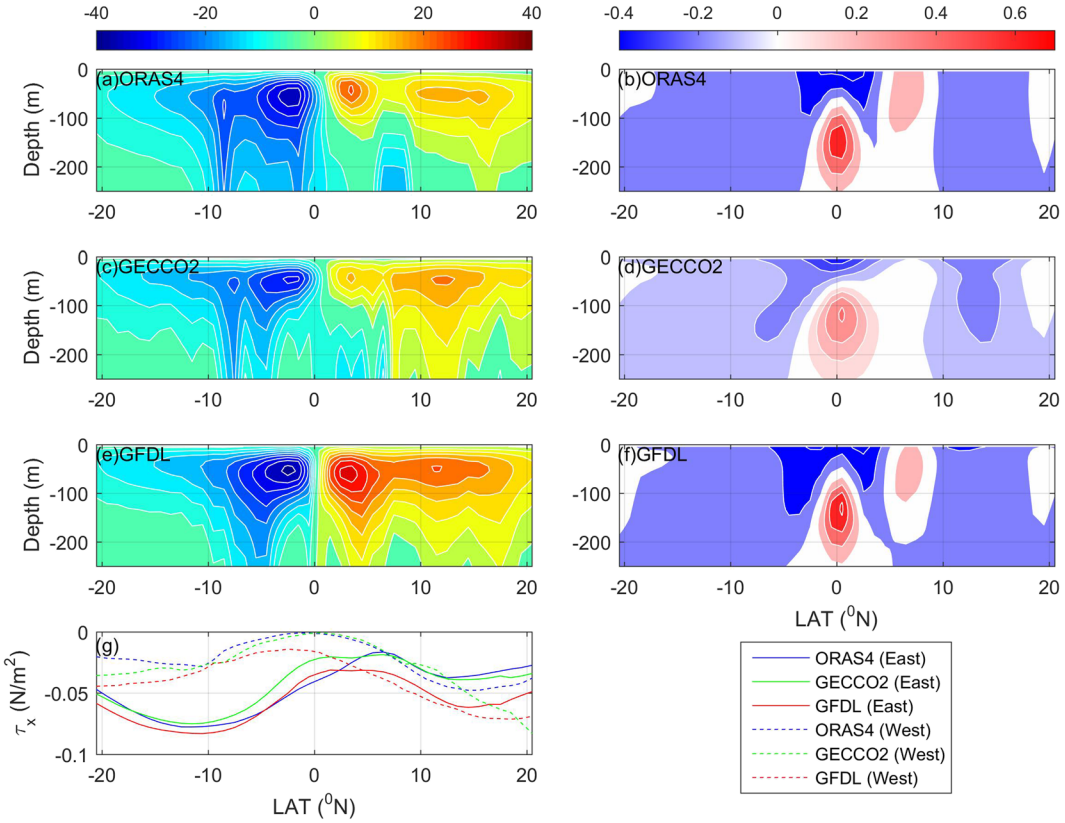

Figure 4. Time mean (1961–2010) meridional overturning stream function depicting the Pacific subtropical-tropical cells (Sv, positive clockwise and negative counterclockwise) and zonal current speeds (m/s) at 160.5°W in the tropical Pacific Ocean in (a and b) ORAS4, (c and d) GECCO2, and (e and f) GFDL. (g) Time mean zonal wind profile in the western and eastern Pacific averaged between longitude limits of WEP and EEP, respectively (see text).

TCs and weakening of the NSTC (Figure 6g). In GECCO2, trends in the TCs and STCs are considerably weak compared to those of ORAS4 and GFDL. The STCs carry subsurface pycnocline waters equatorward mainly as western boundary currents after circulating across the basin (Lu et al., 1998; Schott et al., 2004) and join the EUC in the west (Lu & McCreary, 1995). The strength of STCs can be inferred from geostrophy (Lee, 2004), and strengthening of STC is marked by anomalous rising and falling of sea surface height in the western and eastern Pacific, respectively (Feng et al., 2010). The resulting east–west gradient anomaly in sea surface height strengthens the EUC. Moreover, the EUC exists due to the east–west gradient in sea level sustained by equatorial easterlies, and it disappears in the absence of easterlies (McCreary & Lu, 1994). Unlike the STC, TC exists due to diapycnal mixing and much of the TC waters converge toward the equator and feeds the EUC in the interior ocean (mainly in central and eastern Pacific) and away from western boundary (Lu et al., 1998). According to Nie et al. (2019), the major source of EUC waters comes through the western boundary pathway and the TCs only contribute 22% of the EUC. Hence, trends in EUC are expected to reflect the STC strengths. As expected, the trends in EUCs in the three products are consistent with the trends in their STCs. In ORAS4 (GFDL), there is a strengthening (weakening) of southern (northern) STC (Figures 6a, 6g, S8a, and S8d) with an accelerating (decelerating) EUC (Figures 6b and 6g). The weak trends in TCs and STCs of GECCO2 are also manifested as a weak acceleration in its EUC. In all three products, the trends in their respective EUC are reflected in the subsurface cooling trends in the east (Figures 6c, 6f, and 6i).

In the eastern Pacific, in all products, the subsurface cooling trends are centered approximately between 100 and 120 m along the thermocline (20°C isotherm) between 140 and 130°W (220–230°E in Figures 6c, 6f, and 6i), which is under the Niño3.4 region. For convenience, we define this location as the origin of cooling (OC). The cooling trend is strongest in ORAS4 with the cooling extending both westward and eastward from the

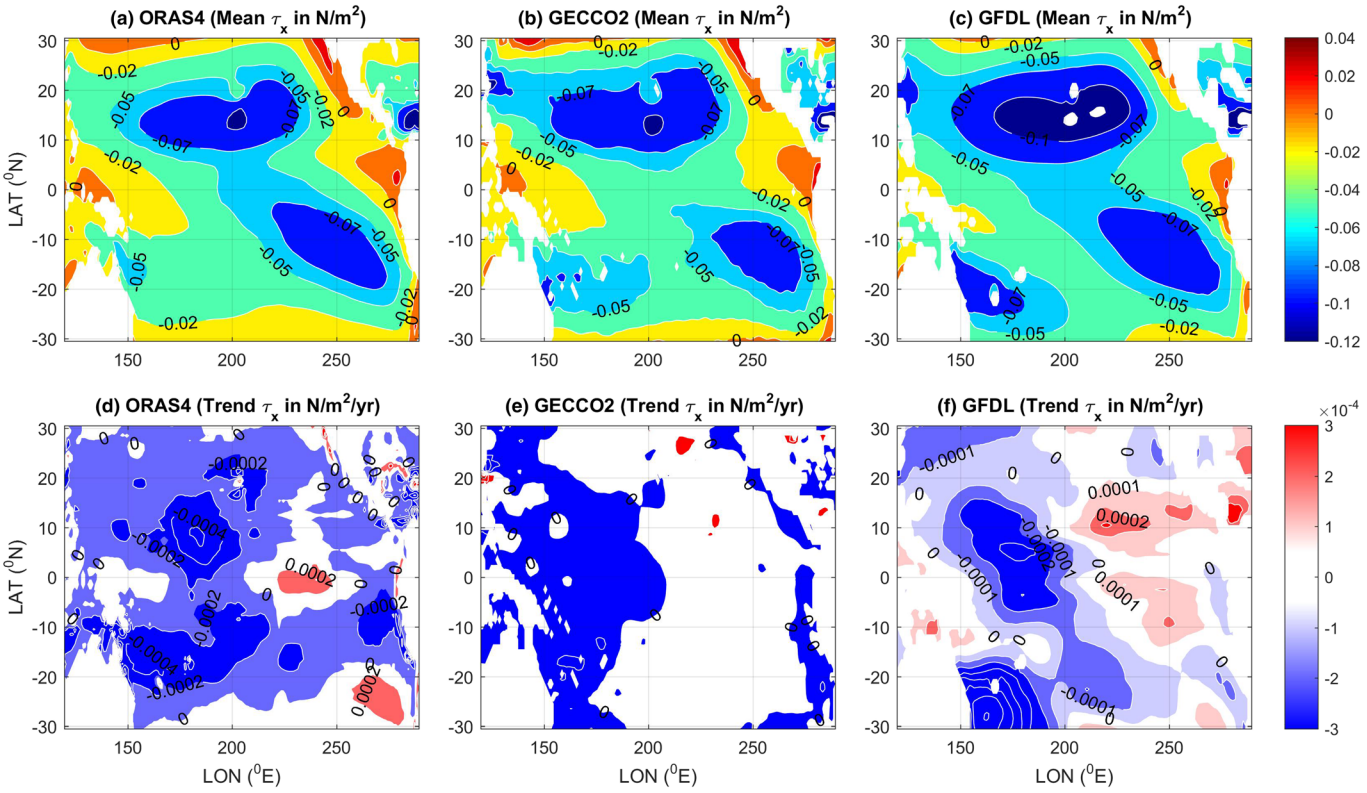

Figure 5. Time mean (1961–2010) zonal wind stress and its trend in the tropical Pacific Ocean in (a and d) ORAS4, (b and e) GECCO2, and (c and f) GFDL.

OC along the thermocline with only a negligible decline in its magnitude. The cooling trend in ORAS4 also extends up to the surface layers in the east. In GECCO2, toward east of the OC, the cooling declines rapidly along the thermocline and transitions to a subsurface warming above the thermocline in EEP. Toward west of the OC, the decline in cooling along the thermocline is not as rapid and there is a weak cooling trend along the deeper thermocline layers of the western Pacific. In GFDL, the cooling trend in OC is really weak and it declines quite rapidly both eastwards and westwards. However, a strong and confined cooling can be observed along the deeper thermocline of the western Pacific (Figure 6i).

The trends in temperature tendencies due to horizontal advection and all the remaining terms of the heat budget are shown in Figure 7. Though the trends are inconsistent across the reanalysis products, the mean values of the temperature tendencies shown in Figure 7 are consistent across them (Figure S9). In ORAS4 and GECCO2, the horizontal advection is warming the layers immediately above the thermocline and cooling the layers beneath (Figures 7a, 7b, 7d, and 7e). This could be attributed to the strengthening of EUC, where, in layers above the thermocline, warm waters within the thermocline from the western Pacific are transported eastwards. In layers below the thermocline, cool deeper waters are transported eastwards. In ORS4, a basin-wide westward acceleration of equatorial waters is noticed (Figure S10b), while in GECCO2, this westward acceleration is limited to 100 to 250°E (Figure S10e). This must be the reason for a basin-wide cooling along thermocline in ORAS4 and the observed cooling within the above-mentioned longitudes in GECCO2. The cooling of layers above the thermocline can be explained by the remaining terms that include vertical advection and mixing (Figures 7c and 7f). The patches of trends in temperature tendencies, thermocline, and isopycnals all run nearly parallel, and this suggests that cross-isopycnal mixing is the dominant mechanism here. Corroborating this, the trends in Brunt-Vaisala frequency (N^2) of the surface layers of ORAS4 show a decrease in stability (Figure S11b). In GECCO2, such noticeable decreasing trends in N^2 are confined to surface layers of the east (Figure S11d).

In GFDL, the EUC weakens, and this is manifested as cooling in layers above the thermocline (Figure 7g). However, quite similar to GECCO2 and ORAS4, in GFDL, the layers below the thermocline also cool due to

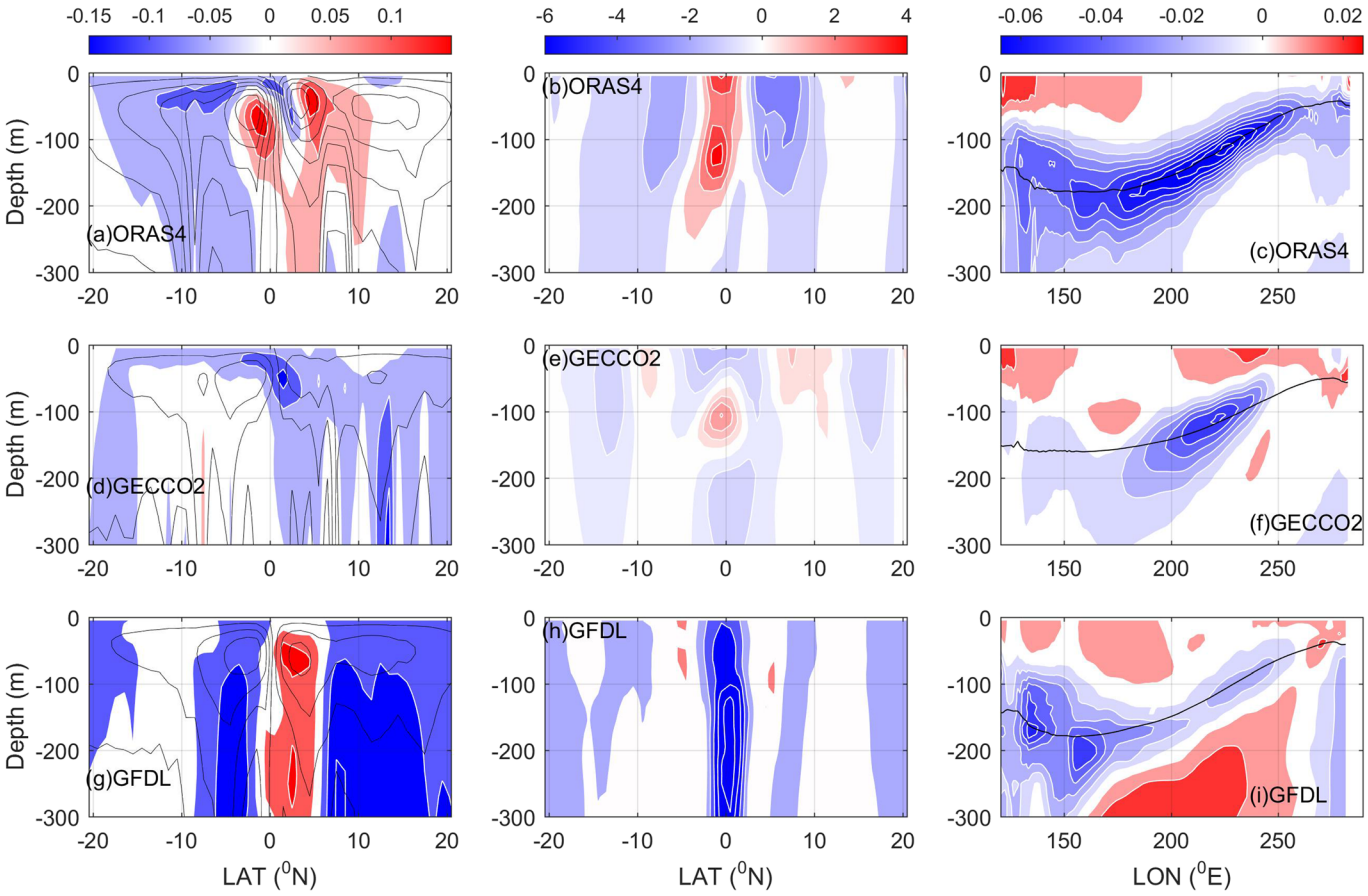

Figure 6. Trends (1961–2010) in meridional overturning stream function depicting the subtropical-tropical cells (Sv/year, positive clockwise and negative counterclockwise), zonal current speeds (cm/s/decade) at 160.5°W and the equatorial subsurface temperature (°C/year) in (a–c) ORAS4, (d–f) GECCO2, and (g–i) GFDL. A qualitative representation of mean cell strength contours (black) is also shown in the first column, and the profile of mean thermocline depth (black line) is shown in the last column.

zonal advection. In this regard, the trends in equatorial zonal velocities in GFDL show basin-wide westward acceleration in the layers above 400-m depth and strong eastward acceleration in the layers below (Figure S10h). Hence, the eastward accelerated cooler waters of layers deeper than 400 m could be supplying the westward accelerated waters above them in the east. The cooling below the thermocline could be due to this vertical structure of zonal currents. The remaining terms of the heat budget that account for mixing and vertical advection show strong warming along the thermocline (Figure 7i). The trends in N^2 also show increasing stability in the region (Figure S11h). This can explain the weak cooling in GFDL along the eastern equatorial thermocline. An interesting observation here is that, in GFDL, layers deeper than the thermocline show a warming trend (Figure 6i). Understanding the mechanism behind such trends demands a more detailed analysis with exact HFs, mixing coefficients, and vertical velocities, which is beyond the scope of this paper. However, in this regard, we once again highlight the strong trends in zonal velocities of the deeper layers (down to 1,000 m) of equatorial Pacific in GFDL (Figure S10h) and negative trends in N^2 in its deep layers (Figure S11h). This could be due to the stronger easterlies (Figure S12) in GFDL and potentially related to other processes such as vertical or diapycnal mixing.

Returning to HF and OD contributions to SST trends in EEP, in all three products, the trends in subsurface temperature as well as SST are consistent with the known mechanisms related to temperature variability linking STCs, EUC, and surface HFs. Hence, the inference made from ML heat budget analysis can be considered valid, at least qualitatively. The differences in these reanalyses point toward the paramount importance of surface heat and momentum fluxes which themselves are related to the coupled dynamics that

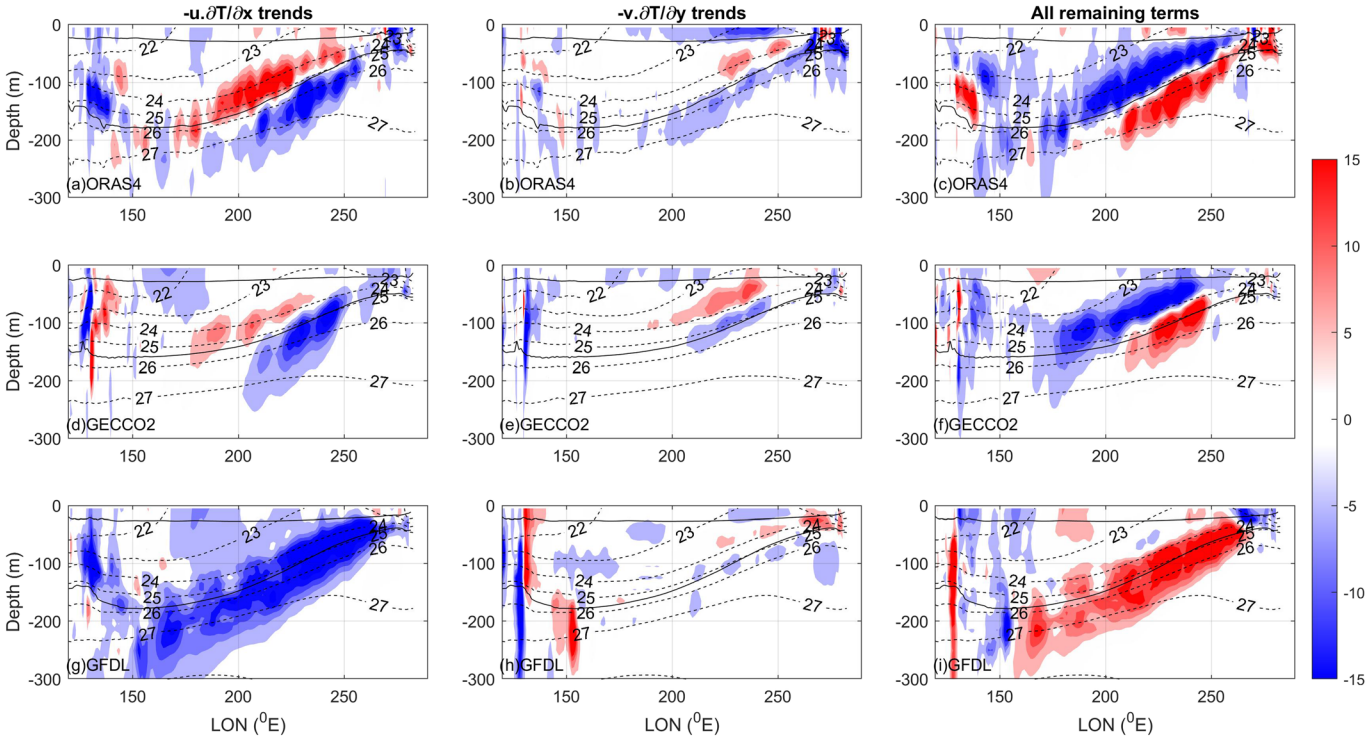

Figure 7. Trends (1961–2010) in temperature tendencies (°C/year/century) due to zonal advection, (a) ORAS4, (d) GECCO2, and (g) GFDL; meridional advection, (b) ORAS4, (e) GECCO2, and (h) GFDL; and all remaining terms in the heat budget, (c) ORAS4, (f) GECCO2, and (i) GFDL. Broken lines represent density (density: 1,000 kg/m^3) contours, and solid lines represent thermocline depth (between 50 and 200 m) and mixed layer depth (below surface within 40 m).

determine the extent of warming in the EEP. This shows that data assimilation is only effective when complemented by accurate surface flux forcings. This also suggests that the usage of reanalysis products as a proxy for observations cannot guarantee a reliable representation of reality. Hence, in studies involving reanalysis products, it is better to compare them based on the specific objective of the study and handpick the most suitable one(s).

4.2. ITF and Upper Layer HCA

The equatorial Pacific SST gradient, the EEP heat uptake, and related upper layer ODs have been extensively studied (England et al., 2014; Kosaka & Xie, 2013) for the global warming hiatus period (1998–2013). The slowdown in global warming for a decade is debated, but the main mechanism invoked is related to the heat uptake by the ocean in the ECT. A model study focused on the heat content of the upper 700 m shows that during this period, a major share of increased heat uptake by the Pacific due to strengthened easterlies is advected into Indian Ocean through strengthened Indonesian Throughflow (ITF). The strengthening of easterlies in the northwestern tropical Pacific is identified as the cause for the strengthening of ITF (Lee et al., 2015). Since ITF is a part of the global conveyer belt that also facilitates thermal coupling of the Indo-Pacific basins, we investigate ITF in the reanalysis products (Text S13 and Figure S13). In GFDL, the high mean easterlies in the northwestern Pacific and their increasing trends result in a strong ITF with a strong increasing trend. Similarly, in ORAS4, a weaker increasing trend in ITF is observed with the increase in the easterlies of its tropical northwestern Pacific. However, in GECCO2, ITF decreases despite an increasing trend in the easterlies. Unlike ORAS4 and GFDL, in GECCO2, the tropical southern Indian Ocean sea level rises, and this downstream control of ITF appears to be dominant in governing its strength. The rising trend in southeastern tropical Indian Ocean sea level in GECCO2 when compared to ORAS4 is also reported in Jayasankar, Eldho, et al. (2019). As per Jayasankar, Murtugudde, and Eldho (2019), unlike GFDL and ORAS4, there is a deepening trend in thermocline depth of the tropical southern Indian Ocean in GECCO2 in response to its declining Indian Ocean deep meridional overturning circulation (MOC). The impact of the deep MOC on the upper thermocline is in accord with theoretical

expectations (Boccaletti, 2005; Boccaletti et al., 2004, 2005). Considering the recently reported results that the Indian Ocean warming may affect the Pacific response to global warming (Zhang et al., 2019), the differences in the Indian Ocean in the three reanalysis products must be assessed critically (Jayasankar, Murtugudde, & Eldho, 2019). Jayasankar, Eldho, et al. (2019) have shown that ITF in ORAS4 is more realistic than that in GECCO2 and the ITF in GFDL shows unrealistic trends. Since ITF trends in these products can be explained by the trends and means of their wind stresses, it gives us more confidence in the realism of ECMWF winds that are used to force ORAS4. Regarding the heat content anomaly (HCA) of the upper 700 m, all three products capture the seasonality of the HCA in the Pacific Ocean (Text S14 and Figure S14). However, the decadal evolution of the HCA in each product is different due to the different initial conditions. Deconvolving the role of ITF and local winds in the upper layer heat content variability is not straightforward, and thus, this brief discussion on the differences in the reanalysis products must suffice here.

5. Summary and Conclusions

The equatorial zonal SST gradient (Δ_{EW}SST) in the Pacific and its strong relation with the zonal winds and heat uptake in the EEP have a large influence on global climate at seasonal to interannual timescales. The heat uptake in the EEP is also shown to have a major influence on the atmospheric warming due to anthropogenic greenhouse gas emissions. The EEP features the eastern Pacific cold tongue (ECT) which is characterized by a sustained year-round upwelling, is relatively cooler, and is a location of strong heat uptake. The SST variability in the EEP largely determines the Δ_{EW}SST variability, because SST is less variable in the warm WEP. However, atmospheric convection over the warm, fresh pool in the WEP plays a significant role in the coupled feedbacks that control the zonal SST gradient. Climate models have a chronic Pacific ECT cold bias which will impact the future climate projections. The evaluation of the ODs of the equatorial Pacific Ocean in the climate models demands high-quality reanalysis products and observations to validate against. Hence, we have evaluated three ocean reanalysis products (ORAS4, GECCO2, and GFDL) for their trends (from 1961 to 2010) in Niño3.4 SST and Δ_{EW}SST and the ODs that contribute to the SST trends in each of them.

The SST trends in the Pacific Ocean in four observational data sets (HadISST, ERSST, Kaplan SST, and COBE2) are first compared. HadISST shows an increasing trend in Δ_{EW}SST while the other three show weak and insignificant trends. The spatial pattern of the Pacific Ocean SST trend in HadISST is also remarkably different from that of the other three data sets. However, the inconsistencies in SST trends among the SST products are mainly concentrated in the EEP. Among the reanalysis products, the spatial pattern of SST trend in observational data sets is captured well by ORAS4, and in the EEP, it is more in line with HadISST data set. Spatial correlation between SST products and reanalysis products also shows the credibility of ORAS4 over the other two reanalyses. Both ORAS4 and GFDL show an increasing trend in Δ_{EW}SST while GECCO2 displays a weakening trend. This is due to a strong warming trend in the EEP and Niño3.4 SSTs of GECCO2 compared to those of ORAS4 and GFDL. As the initial conditions of each product also play a role in Niño3.4 SST trends, it is not possible to differentiate model biases from the influence of initial conditions. However, when Δ_{EW}SST is evaluated, the errors due to initial conditions are expected to somewhat diminish to achieve a better representation of the equatorial SST. The trend in Niño3.4 SST in observational products is also not as strong as their respective warming trends in WEP and EEP SSTs. This is clear from the spatial patterns of SST trends of each. This could be an indication of the increasing influence of a comparatively cooler EEP on the Niño3.4 region. If confirmed, this can be used to elucidate the nature of Δ_{EW}SST trends in the real world. Models which capture the observed role of EEP and WWP in the SST gradient and its trend can yield further insights into the future of oceanic heat uptake as well as other important issues such as the response of ENSO and its diversity in a warming world. In this regard, ORAS4 captures the observed SST trend patterns remarkably well and the ITF in this product is more realistic. This increases the confidence in the model and surface fluxes that are used to force the model. These also provide strong supporting evidence that Δ_{EW}SST has increased in the last five decades.

To differentiate surface flux and OD contributions to the SST trends, an ML heat budget analysis is performed. In all products, ML mean temperature trends in key regions (WEP, Niño3.4, and EEP) closely match their respective SST trends. GFDL is a coupled climate model where the HFs predicted by the model are constrained by the NCEP fluxes and the exact HFs by which it is forced are not available. Therefore, NCEP

fluxes themselves are used for ML heat budget analysis in GFDL. For the Niño3.4 region, there are differences in mean HF across the products, but the trends in HF in all are increasing. For WEP and EEP in GFDL, the HF contributions are cooling over time. This is likely due to the change of atmospheric products used in GFDL from NCEP/NCAR data set to NCEP/DOE data set after 1978 with the mean of the latter being lower than the former. Consequently, in EEP, the HF (OD) contribution is cooling (warming) in GFDL. To summarize, in EEP, all three products show different trends in HF and OD contributions; HF contributions show a strong warming in ORAS4, an insignificant cooling trend in GECCO2 and a cooling trend in GFDL. The respective trends in OD contributions are more or less the inverse of the HF contributions. The ML heat budget analysis thus suggests that the HF and ODs that deliver the respective EEP SST trends in these reanalysis products are inconsistent. The respective strong cooling and warming trends in OD contributions of ORAS4 and GFDL in EEP are mainly governed by the residual term that account for mixing.

The upper layer meridional overturning cells (STCs and TCs) and EUC are investigated further for their role at decadal timescales. The mean structure of TCs, STCs, and EUC as well as the seasonality of TCs and STCs in the reanalyses internally are consistent with each other. However, the mean NTC, NSTC, and mean EUC of GFDL are stronger than those of ORAS4 and GECCO2. The EUC in GECCO2 is the weakest. The spatial pattern of mean zonal wind stress in the three products can explain their respective mean strengths of TCs, STCs, and EUC. The easterlies of GFDL are the strongest, driving the strengths of its upper layer meridional overturning cells. In terms of trends, the northern (southern) STC in GFDL (ORAS4) spins down (up). However, only weak trends are present in GECCO2. Corresponding to the trends in wind stress, strong deceleration (acceleration) of the EUC occurs in GFDL (ORAS4) while a weak acceleration of the same occurs in GECCO2. The trend in the EUC strength of each product is reflected in its equatorial (a latitude band of 3°) subsurface temperature trend.

A strong cooling all along the thermocline from east to west with a maximum cooling below the Niño3.4 region is evident in ORAS4 while a weak and zonally limited cooling occurs along the thermocline in GECCO2. In GFDL, this cooling is the weakest among the three below the Niño3.4 region, but a strong cooling is evident deeper in the western Pacific along with a basin-wide warming in deeper layers below the thermocline. The trends in TCs, STCs, EUC, and subsurface temperatures are quite internally consistent with the zonal wind stress trends in each product. A weakening (strengthening) of easterlies is observed in the eastern (western) Pacific in GFDL. A strengthening of easterlies is observed in ORAS4 except for the Niño3.4 region and its vicinity. However, a relatively weak strengthening of zonal easterlies is observed in GECCO2 which is confined to the western Pacific. Therefore, the ODs of the reanalysis products evaluated and their respective forcings like wind stresses and HFs qualitatively support the inferences drawn from the ML heat budget analysis. This underscores the lack of agreement between the trends in Niño3.4 SST, Δ_{EW}SST, and ODs in these products. Hence, evaluation of climate models just by comparing trends of these simple indices could result in wrong inferences of their dynamics and reliability.

In this study, we have shown that the monthly zonal SST gradient trends of the equatorial Pacific Ocean reproduced in two reanalysis products from 1961 to 2010 are similar (ORAS4 and GFDL) albeit supported by different trends in ODs. This suggests that when the accuracy in forcing fluxes of models is compromised, data assimilation and other constraints such as flux corrections could guide the model dynamics through unnatural pathways such that the observed trends and climatology are captured for the wrong reasons. Hence, accurate forcing fluxes maybe the most critically needed quantities to improve ocean reanalyses where there are potentially multiple pathways by which observed trends can be generated in the complex atmosphere-ocean dynamics system. Ocean dynamical processes also must be accurately represented in reanalyses if they are to serve as reliable validation products for climate models and for advancing process understanding of physical mechanisms. The inconsistencies identified here suggest that taking an ensemble average of reanalysis products as a proxy for past climate may result in misleading conclusions. Further, ocean reanalysis products must make available all forcings, variables, and diffusivities so that rigorous evaluations of them can be carried out.

Data Availability Statement

The ocean reanalysis data sets (GECCO2, ORAS4, and GFDL) and respective wind data sets are downloaded from links available from the University of Hamburg website (https://icdc.cen.uni-hamburg.de/daten.html).

HadISST data set is downloaded from UK Met Office website (https://www.metoffice.gov.uk/hadobs/hadisst/). ERSST, Kaplan SST, COBE2, and NCEP heat fluxes provided by NOAA/OAR/ESRL PSD, Boulder, Colorado, USA, are downloaded from their website (https://www.esrl.noaa.gov/psd/data/gridded/). The ECMWF winds are downloaded from ECMWF website (http://apps.ecmwf.int/datasets/).

Acknowledgments
We acknowledge the computational resources provided by the Indian Institute of Technology, Bombay. We thank the two anonymous reviewers for their suggestions and corrections which helped us to improve the quality of the manuscript. R. M. gratefully acknowledges the Visiting Faculty position at the Indian Institute of Technology, Bombay.

References

Balmaseda, M. A., Mogensen, K., & Weaver, A. T. (2013). Evaluation of the ECMWF ocean reanalysis system ORAS4. *Quarterly Journal of the Royal Meteorological Society*, *139*(674), 1132–1161. https://doi.org/10.1002/qj.2063

Bjerknes, J. (1969). Atmospheric teleconnections from the equatorial Pacific. *Monthly Weather Review*, *97*(3), 163–172. https://doi.org/10.1175/1520-0493(1969)097<0163:ATFTEP>2.3.CO;2

Boccaletti, G. (2005). Timescales and dynamics of the formation of a thermocline. *Dynamics of Atmospheres and Oceans*, *39*(1–2), 21–40. https://doi.org/10.1016/j.dynatmoce.2004.10.010

Boccaletti, G., Pacanowski, R. C., George, S., & Philander, H. (2005). A diabatic mechanism for decadal variability in the tropics. *Dynamics of Atmospheres and Oceans*, *39*(1–2), 3–19. https://doi.org/10.1016/j.dynatmoce.2004.10.009

Boccaletti, G., Pacanowski, R. C., George, S., Philander, H., & Fedorov, A. V. (2004). The thermal structure of the upper ocean. *Journal of Physical Oceanography*, *34*(4), 888–902. https://doi.org/10.1175/1520-0485(2004)034<0888:TTSOTU>2.0.CO;2

Cai, W., Wang, G., Dewitte, B., Wu, L., Santoso, A., Takahashi, K., et al. (2018). Increased variability of eastern Pacific El Niño under greenhouse warming. *Nature*, *564*(7735), 201–206. https://doi.org/10.1038/s41586-018-0776-9

Cane, M. A., Clement, A. C., Kaplan, A., Kushnir, Y., Pozdnyakov, D., Seager, R., et al. (1997). Twentieth-century sea surface temperature trends. *science*, *275*(5302), 957–960. https://doi.org/10.1126/science.275.5302.957

Chang, Y.-S., Zhang, S., Rosati, A., Delworth, T. L., & Stern, W. F. (2013). An assessment of oceanic variability for 1960–2010 from the GFDL ensemble coupled data assimilation. *Climate Dynamics*, *40*(3–4), 775–803. https://doi.org/10.1007/s00382-012-1412-2

Clement, A. C., Seager, R., Cane, M. A., & Zebiak, S. E. (1996). An ocean dynamical thermostat. *Journal of Climate*, *9*(9), 2190–2196. https://doi.org/10.1175/1520-0442(1996)009<2190:AODT>2.0.CO;2

Coats, S., & Karnauskas, K. B. (2018). A role for the equatorial undercurrent in the ocean dynamical thermostat. *Journal of Climate*, *31*(16), 6245–6261. https://doi.org/10.1175/JCLI-D-17-0513.1

Collins, M., An, S.-I., Cai, W., Ganachaud, A., Guilyardi, E., Jin, F.-F., et al. (2010). The impact of global warming on the tropical Pacific Ocean and El Niño. *Nature Geoscience*, *3*(6), 391–397. https://doi.org/10.1038/ngeo868

Dee, D. P., Uppala, S. M., Simmons, A. J., Berrisford, P., Poli, P., Kobayashi, S., et al. (2011). The ERA-Interim reanalysis: Configuration and performance of the data assimilation system. *Quarterly Journal of the Royal Meteorological Society*, *137*(656), 553–597. https://doi.org/10.1002/qj.828

Delworth, T. L., Zeng, F., Rosati, A., Vecchi, G. A., & Wittenberg, A. T. (2015). A link between the hiatus in global warming and North American drought. *Journal of Climate*, *28*(9), 3834–3845. https://doi.org/10.1175/JCLI-D-14-00616.1

Dong, S., Gille, S. T., & Sprintall, J. (2007). An assessment of the Southern Ocean mixed layer heat budget. *Journal of Climate*, *20*(17), 4425–4442. https://doi.org/10.1175/JCLI4259.1

Drenkard, E. J., & Karnauskas, K. B. (2014). Strengthening of the Pacific equatorial undercurrent in the SODA reanalysis: Mechanisms, ocean dynamics, and implications. *Journal of Climate*, *27*(6), 2405–2416. https://doi.org/10.1175/JCLI-D-13-00359.1

England, M. H., McGregor, S., Spence, P., Meehl, G. A., Timmermann, A., Cai, W., et al. (2014). Recent intensification of wind-driven circulation in the Pacific and the ongoing warming hiatus. *Nature Climate Change*, *4*(3), 222–227. https://doi.org/10.1038/nclimate2106

Feng, M., McPhaden, M. J., & Lee, T. (2010). Decadal variability of the Pacific subtropical cells and their influence on the southeast Indian Ocean. *Geophysical Research Letters*, *37*, L09606. https://doi.org/10.1029/2010GL042796

Hendon, H. H. (2003). Indonesian rainfall variability: Impacts of ENSO and local air-sea interaction. *Journal of Climate*, *16*(11), 1775–1790. https://doi.org/10.1175/1520-0442(2003)016<1775:IRVIOE>2.0.CO;2

Hirahara, S., Ishii, M., & Fukuda, Y. (2014). Centennial-scale sea surface temperature analysis and its uncertainty. *Journal of Climate*, *32*.

Huang, B., Thorne, P. W., Banzon, V. F., Boyer, T., Chepurin, G., Lawrimore, J. H., et al. (2017). Extended reconstructed sea surface temperature, version 5 (ERSSTv5): Upgrades, validations, and intercomparisons. *Journal of Climate*, *30*(20), 8179–8205. https://doi.org/10.1175/JCLI-D-16-0836.1

Jayasankar, T., Eldho, T. I., Ghosh, S., & Murtugudde, R. (2019). Assessment of the interannual variability of local atmospheric and ITF contribution to the subsurface heat content of southern tropical Indian Ocean in GECCO2 and ORAS4 using ROMS. *Global and Planetary Change*, *181*, 102974. https://doi.org/10.1016/j.gloplacha.2019.05.014

Jayasankar, T., Murtugudde, R., & Eldho, T. I. (2019). The Indian Ocean deep meridional overturning circulation in three ocean reanalysis products. *Geophysical Research Letters*, *46*(21), 12,146–12,155. https://doi.org/10.1029/2019GL084244

Jerlov, N. (1968). *Optical Oceanography* (p. 199). Amsterdam, The Netherlands: Elsevier.

Kalnay, E., Kanamitsu, M., Kistler, R., Collins, W., Deaven, D., Gandin, L., et al. (1996). The NCEP/NCAR 40-year reanalysis project. *Bulletin of the American Meteorological Society*, *77*(3), 437–471. https://doi.org/10.1175/1520-0477(1996)077<0437:TNYRP>2.0.CO;2

Kanamitsu, M., Ebisuzaki, W., Woollen, J., Yang, S.-K., Hnilo, J. J., Fiorino, M., & Potter, G. L. (2002). NCEP-DOE AMIP-II reanalysis (R-2). *Bulletin of the American Meteorological Society*, *83*(11), 1631–1644. https://doi.org/10.1175/BAMS-83-11-1631

Kaplan, A., Cane, M. A., Kushnir, Y., Clement, A. C., Blumenthal, M. B., & Rajagopalan, B. (1998). Analyses of global sea surface temperature 1856–1991. *Journal of Geophysical Research*, *103*(C9), 18,567–18,589. https://doi.org/10.1029/97JC01736

Karnauskas, K. B., Seager, R., Kaplan, A., Kushnir, Y., & Cane, M. A. (2009). Observed strengthening of the zonal sea surface temperature gradient across the equatorial Pacific Ocean. *Journal of Climate*, *22*(16), 4316–4321. https://doi.org/10.1175/2009JCLI2936.1

Kennedy, J. J., Rayner, N. A., Smith, R. O., Parker, D. E., & Saunby, M. (2011a). Reassessing biases and other uncertainties in sea surface temperature observations measured in situ since 1850: 1. Measurement and sampling errors. *Journal of Geophysical Research*, *116*.

Kennedy, J. J., Rayner, N. A., Smith, R. O., Parker, D. E., & Saunby, M. (2011b). Reassessing biases and other uncertainties in sea surface temperature observations measured in situ since 1850: 2. Biases and homogenization. *Journal of Geophysical Research*, *116*.

Kohl, A. (2015). Evaluation of the GECCO2 ocean synthesis: Transports of volume, heat and freshwater in the Atlantic. *Quarterly Journal of the Royal Meteorological Society*, *141*(686), 166–181. https://doi.org/10.1002/qj.2347

Kosaka, Y., & Xie, S.-P. (2013). Recent global-warming hiatus tied to equatorial Pacific surface cooling. *Nature*, *501*(7467), 403–407. https://doi.org/10.1038/nature12534

Lee, S.-K., Park, W., Baringer, M. O., Gordon, A. L., Huber, B., & Liu, Y. (2015). Pacific origin of the abrupt increase in Indian Ocean heat content during the warming hiatus. *Nature Geoscience*, *8*(6), 445–449. https://doi.org/10.1038/ngeo2438

Lee, T. (2004). Decadal weakening of the shallow overturning circulation in the South Indian Ocean. *Geophysical Research Letters*, *31*(22), L22302. https://doi.org/10.1029/2004GL021774

Li, G., & Xie, S.-P. (2014). Tropical biases in CMIP5 multimodel ensemble: The excessive equatorial Pacific cold tongue and double ITCZ problems. *Journal of Climate*, *27*(4), 1765–1780. https://doi.org/10.1175/JCLI-D-13-00337.1

Liu, Z. (1994). A simple model of the mass exchange between the subtropical and tropical ocean. *Journal of Physical Oceanography*, *24*(6), 1153–1165. https://doi.org/10.1175/1520-0485(1994)024<1153:ASMOTM>2.0.CO;2

Lohmann, K., & Latif, M. (2005). Tropical Pacific decadal variability and the subtropical-tropical cells. *Journal of Climate*, *18*(23), 5163–5178. https://doi.org/10.1175/JCLI3559.1

Lu, P., & McCreary, J. P. Jr. (1995). Influence of the ITCZ on the flow of thermocline water from the subtropical to the equatorial Pacific Ocean. *Journal of Physical Oceanography*, *25*(12), 3076–3088. https://doi.org/10.1175/1520-0485(1995)025<3076:IOTIOT>2.0.CO;2

Lu, P., McCreary, J. P. Jr., & Klinger, B. A. (1998). Meridional circulation cells and the source waters of the Pacific equatorial undercurrent. *Journal of Physical Oceanography*, *28*(1), 62–84. https://doi.org/10.1175/1520-0485(1998)028<0062:MCCATS>2.0.CO;2

McCreary, J. P. Jr., & Lu, P. (1994). Interaction between the subtropical and equatorial ocean circulations: The subtropical cell. *Journal of Physical Oceanography*, *24*, 466–497.

McPhaden, M. J., & Zhang, D. (2002). Slowdown of the meridional overturning circulation in the upper Pacific Ocean. *Nature*, *415*(6872), 603–608. https://doi.org/10.1038/415603a

McPhaden, M. J., & Zhang, D. (2004). Pacific Ocean circulation rebounds. *Geophysical Research Letters*, *31*, L18301. https://doi.org/10.1029/2004GL020727

Murtugudde, R., Beauchamp, J., McClain, C. R., Lewis, M., & Busalacchi, A. J. (2002). Effects of penetrative radiation on the upper tropical ocean circulation. *Journal of Climate*, *15*(5), 470–486. https://doi.org/10.1175/1520-0442(2002)015<0470:EOPROT>2.0.CO;2

Nie, X., Gao, S., Wang, F., Chi, J., & Qu, T. (2019). Origins and pathways of the Pacific equatorial undercurrent identified by a simulated adjoint tracer. *Journal of Geophysical Research: Oceans*, *124*, 2331–2347. https://doi.org/10.1029/2018JC014212

Paulson, C. A., & Simpson, J. J. (1977). Irradiance measurements in the upper ocean. *Journal of Physical Oceanography*, *7*(6), 952–956. https://doi.org/10.1175/1520-0485(1977)007<0952:IMITUO>2.0.CO;2

Qiu, B., & Kelly, K. A. (1993). Upper-ocean heat balance in the Kuroshio Extension region. *Journal of Physical Oceanography*, *23*(9), 2027–2041. https://doi.org/10.1175/1520-0485(1993)023<2027:UOHBIT>2.0.CO;2

Ray, S., Wittenberg, A. T., Griffies, S. M., & Zeng, F. (2018a). Understanding the equatorial Pacific cold tongue time-mean heat budget. *Part I: Diagnostic framework. Journal of Climate*, *31*, 9965–9985.

Ray, S., Wittenberg, A. T., Griffies, S. M., & Zeng, F. (2018b). Understanding the equatorial Pacific cold tongue time-mean heat budget. *Part II: Evaluation of the GFDL-FLOR coupled GCM. Journal of Climate*, *31*, 9987–10,011.

Schott, F. A., Mccreary, J. P., & Johnson, G. C. (2004). Shallow overturning circulations of the tropical-subtropical oceans. Earth climate: The ocean-atmosphere interaction. *Geophys Monograph*, *147*, 261–304.

Seager, R., Cane, M., Henderson, N., Lee, D.-E., Abernathey, R., & Zhang, H. (2019). Strengthening tropical Pacific zonal sea surface temperature gradient consistent with rising greenhouse gases. *Nature Climate Change*, *9*(7), 517–522. https://doi.org/10.1038/s41558-019-0505-x

Seager, R., & Murtugudde, R. (1997). Ocean dynamics, thermocline adjustment, and regulation of tropical SST. *Journal of Climate*, *10*(3), 521–534. https://doi.org/10.1175/1520-0442(1997)010<0521:ODTAAR>2.0.CO;2

Sen, P. K. (1968). Estimates of the regression coefficient based on Kendall's tau. *Journal of the American Statistical Association*, *63*(324), 1379–1389. https://doi.org/10.1080/01621459.1968.10480934

Simpkins, G. (2017). Progress in climate modelling. *Nature Climate Change*, *7*(10), 684–685. https://doi.org/10.1038/nclimate3398

Sun, D.-Z., & Liu, Z. (1996). Dynamic ocean-atmosphere coupling: A thermostat for the tropics. *Science*, *272*(5265), 1148–1150. https://doi.org/10.1126/science.272.5265.1148

Theil, H. (1950). A rank-invariant method of linear and polynomial regression analysis, I, II, III, Nederl. Akad. Wetensch., Proc., 53, 386–392, 521–525, 1397–1412.

Trenberth, K. E., Branstator, G. W., Karoly, D., Kumar, A., Lau, N.-C., & Ropelewski, C. (1998). Progress during TOGA in understanding and modeling global teleconnections associated with tropical sea surface temperatures. *Journal of Geophysical Research*, *103*(C7), 14,291–14,324. https://doi.org/10.1029/97JC01444

Uppala, S. M., Kållberg, P. W., Simmons, A. J., Andrae, U., Bechtold, V. D. C., Fiorino, M., et al. (2005). The ERA-40 re-analysis. *Quarterly Journal of the Royal Meteorological Society*, *131*(612), 2961–3012. https://doi.org/10.1256/qj.04.176

Vecchi, G. A., Clement, A., & Soden, B. J. (2008). Examining the tropical Pacific's response to global warming. *Eos, Transactions American Geophysical Union*, *89*(9), 81–83. https://doi.org/10.1029/2008EO090002

Vecchi, G. A., & Wittenberg, A. T. (2010). El Niño and our future climate: Where do we stand? *Wiley Interdisciplinary Reviews: Climate Change*, *1*, 260–270.

Yamanaka, G., Tsujino, H., Nakano, H., & Hirabara, M. (2015). Decadal variability of the Pacific subtropical cells and its relevance to the sea surface height in the western tropical Pacific during recent decades. *Journal of Geophysical Research: Oceans*, *120*, 201–224. https://doi.org/10.1002/2014JC010190

Zhang, L., Han, W., Karnauskas, K. B., Meehl, G. A., Hu, A., Rosenbloom, N., & Shinoda, T. (2019). Indian Ocean warming trend reduces Pacific warming response to anthropogenic greenhouse gases: An interbasin thermostat mechanism. *Geophysical Research Letters*, *46*, 10,882–10,890. https://doi.org/10.1029/2019GL084088